# Impact of Multiple Radar reflectivity data assimilation on the numerical simulation of a Flash Flood Event during the HyMeX campaign

Ida Maiello[1], Sabrina Gentile[2,1] , Rossella Ferretti[1,3], Luca Baldini[4], Nicoletta Roberto [4], Errico Picciotti[5,1], Pier Paolo Alberoni[6], Frank Silvio Marzano[7,1]

[1]CETEMPS, Department of Physical and Chemical Sciences - University of L'Aquila, L'Aquila, Italy

[2] Institute of Methodologies for Environmental Analysis, CNR IMAA, Potenza, Italy

[3]Danish Meteorological Institute, Copenaghen, Denmark

[4]Institute of Atmospheric Sciences and Climate, CNR ISAC, Roma, Italy

[5]Himet s.r.l, L'Aquila, Italy

[6]Arpa Emilia Romagna - Servizio Idro-Meteo-Clima, Bologna, Italy

[7]Department of Electronic Engineering, Sapienza University of Rome, Rome, Italy

*Correspondence to*: Ida Maiello (ida.maiello@aquila.infn.it)

**Abstract.** An analysis to evaluate the impact of multiple radar reflectivity data with a three dimensional variational (3D-Var) system on a heavy precipitation event is presented. The main goal is to build a regionally-tuned numerical prediction model and decision-support system for civil prevention and protection within the central Italian regions, distinguishing which type of observations (or a combination of several types) is more effective in improving the accuracy of the forecasted rainfall. In that respect, during the first Special Observation Period (SOP1) of HyMeX (Hydrological cycle in the Mediterranean Experiment) campaign several Intensive Observing Periods (IOPs) were launched and nine occurred in Italy. Among them IOP4 is chosen for this study because of its low predictability regarding the exact location and amount of precipitation. This event hit central Italy on 14 September 2012 producing heavy precipitation and causing several damages to buildings, infrastructures and roads. Reflectivity data taken from three C-band Doppler radars running operationally during the event are assimilated using three-dimensional variational (3D-Var) technique to improve high resolution initial conditions. In order to evaluate the impact of the assimilation procedure at different horizontal resolutions and to assess the impact of assimilating reflectivity data from multiple radars, several experiments using Weather Research and Forecasting (WRF) model are performed. Finally, the statistical indexes as accuracy, equitable threat score, false alarm ratio and frequency bias are used to objectively compare the experiments, using rain gauge data as benchmark.

***Keywords:*** *radar data assimilation, WRF, 3D-Var, HyMeX*

## 1 Introduction

In the last few years a large number of floods caused by different meteorological events occurred in Italy. These events mainly affected small areas (few hundreds of square kilometers) making their forecast very difficult. Indeed, one of the

most important factors in producing a flood was found to be the persistence of the meteorological system over the same area allowing for accumulating large amount of rain. In complex orography areas, such the Italian region, this is largely due to the barrier effect produced by the mountains. If precipitation persists over urbanized watersheds with steep slopes, devastating floods can occur in a relatively short time.

The scientific community widely recognizes the need of numerical weather prediction (NWP) models to run at high resolution for improving very short term quantitative precipitation forecasts (QPF) during severe weather events and flash floods. The combination of NWP models and weather radar observations has shown improved skill with respect to extrapolation-based techniques (Sun et al., 2014). Nevertheless, the accuracy of the mesoscale NWP models is negatively affected by the "spin-up" effect (Daley 1991) and is mostly dependent on the errors in the initial and lateral boundary conditions (IC and BC), along with deficiencies in the numerical models themselves, and at the resolution of kilometers even more critical because of the lack of high resolution observations, beside for radar data. Several studies in the meteorological field have demonstrated that the assimilation of appropriate data into the NWP models, especially radar (Sugimoto et al., 2009) and satellite data (Sokol 2009), significantly reduces the "spin-up" effect and improves the IC and BC of the mesoscale models. Classical observations such as TEMP (upper level temperature, humidity, and winds observations) or SYNOP (surface synoptic observations) have not enough density to describe for example local convection, while radar measurements can provide a sufficient density of data. Maiello et al. (2014) showed the positive effect of the assimilation of radar data into the precipitation forecast of a heavy rainfall event in central Italy. The authors showed the gain by using assimilating radar data with respect to the conventional ones. Similar results are obtained for a case of severe convective storm in Croatia by Stanesic and Brewster (2016).

Weather radar has a fundamental role in showing tridimensional structures of convective storms and the associated mesoscale and microscale systems (Nakatani, 2015). Xiao and Sun (2007) showed that, to better predict convective systems, radar observations into NWP models at high resolution (2km) have to be assimilated. Recent researches in the meteorological area have established that the assimilation of real-time data, especially radar measurements (radial velocities and/or reflectivities), into the mesoscale NWP models can better predict precipitations for the next few hours (e.g. Xiao et al., 2005; Sokol and Rezacova, 2006; Dixon et al., 2009; Salonen et al., 2010).

The aim of this study is to investigate the potential of improving NWP rainfall forecasts by assimilating multiple radar reflectivity data in combination or not with conventional observations. This may have a direct benefit also for hydrological applications, particularly for real time flash flood prediction and consequently for civil protection purposes. The novelty of the paper is in exploring impact on the high resolution forecast of the assimilation of multiple radar reflectivity data in a complex orography area, such the Italian region, to predict intense precipitation. This aim is reached by using the IOP4 of the SOP1 of the HyMeX campaign (Ducrocq et al. 2014, Ferretti et al. 2014, Davolio et al. 2015). The SOP1 was held from 5 September to 5 November 2012; the IOP4 was issued for the central Italy target area on 14 September 2012 and it was tagged both as a Heavy Precipitation Event (HPE) and a Flash Flood Event (FFE). Reflectivity from three C-band weather radars is ingested together with traditional meteorological observations (SYNOP and TEMP) using 3D-Var to improve WRF model performance. Several reflectivity data assimilation studies of heavy rainfall cases have been performed (Ha et al. 2011, Das et al. 2015) including with multiple radars data and in complex orography (Lee et al. 2010, Liu et al. 2013), but this is the first experiment conducted on the Italian territory taking advantage of the reflectivity data acquired by the radars that cover central Italy.

The manuscript is arranged as follows. Section 2 provides information on the flash flood event and WRF model configuration. Section 3 presents observations to be assimilated and the WRF 3D-Var data assimilation system. The results are showed and evaluated in the Fourth Section. Summary and conclusions are reflected in the last Section.

## 2 Study area and model set up

Flash floods are still one of the natural hazards producing human and economic losses (Llasat et al. 2013). Moreover, an increasing trend of severe events in the whole Mediterranean area has been found by several authors (Hertig et al. 2012, Martin et al. 2013, Diodato and Bellocchi, 2014). These open issues drove the HyMeX project (http://www.hymex.org) aims at a better understanding of the water cycle in the Mediterranean with focus on extreme weather events. The observation strategy of HyMeX is organized in a long-term (4 years) Enhanced Observation Periods (EOP) and short-term (2 months) Special Observation Periods (SOP). During the SOP1, that was held from 5 September to 5 November 2012 with the major aim of investigating still-unclear mesoscale meteorological mechanisms over the Mediterranean area, three Italian hydro-meteorological site were identified within the Western Mediterranean Target Area (TA): Liguria–Tuscany (LT), northeastern Italy (NEI) and central Italy (CI). Several Intensive Observing Periods (IOPs) were issued during the campaign to document Heavy Precipitation Events (HPE), Flash Floods Events (FFE) and Orographic Precipitation Events (ORP).

### 2.1 Case study

During the day of 14 September 2012 a deep upper level trough entered the Mediterranean basin and deepened over the Tyrrhenian Sea slowly moving south eastward. A cut-off low developed over CI (Figure 1a, c) advecting cold air along the central Adriatic coast producing instability over central and southern Italy, and enhanced the Bora flow over the northern Adriatic Sea. Convection with heavy precipitations occurred in the morning of Friday September 14 mainly along the central eastern Italian coast (Marche and Abruzzo regions), associated with the cut-off low over the Tyrrhenian Sea, producing flood in the urban area of Pescara where rainfall reached 150 mm in a few hours causing several river overflows, a landslide and many damages in the area of the city hospital. Progressive motion south-eastward of the cut-off and its filling (Figure 1b, d) gradually moved phenomena over south of Italy, even if some instability still remained over medium Adriatic until the afternoon of Saturday September 15. At the same time, a ridge developed high pressure on the west part of West Mediterranean domain; this ridge slowly drifts eastwards during the weekend.

Figure 2 shows the interpolated map of 24h accumulated rainfall recorded from rain gauges network from September 14$^{th}$ to September 15$^{th}$ (00:00-00:00UTC) with a maximum accumulated rainfall on the highest peak of Abruzzo region (Campo Imperatore) approximately reaching 300mm in 24 hours. DEWETRA (Italian Civil Protection Department, CIMA Research Foundation, 2014) is an operational platform used by the Italian Civil Protection Department (DPC) and designed by CIMA Research Foundation (http://www.cimafoundation.org/en/) to support operational activities at national or international scale. Rain gauges time series of some selected stations in Marche and Abruzzo regions where most of rainfall is accumulated are presented in Figure 3: Fermo and Pintura di Bolognola (Marche region) respectively with nearly 130 mm/24h (Figure 3a) and 180 mm/24h (Figure 3b); Campo Imperatore, Atri and Pescara Colli (Abruzzo region) with respectively nearly 300mm/24h (Figure 3c), 160 mm/24h (Figure 3d) and 140 mm/24h (Figure 3e). It is clearly shown (Figure 3) that the incremental accumulation started around 02:00UTC of

14th September: in Fermo, Atri and Pescara Colli most of rainfall was concentrated in the first half of the day, whereas in Pintura di Bolognola and Campo Imperatore, precipitation fell all day long. The large amount of hourly precipitation for Atri and Pescara Colli respectively at 06:00UTC and 05:00UTC (red ovals in Fig. 3d and 3e) reaching 45mm/h, indicating convective precipitation, whereas rainfall at Campo Imperatore rain gauge (Fig. 3c) was much weaker but lasting longer which allowed for reaching an accumulated amount of approximately 300mm/24h.

Figure 4 reports a graphical tool that combines the Vertical Maximum Intensity (VMI) reflectivity from the Italian radar network (Vulpiani et al., 2008a) together with the Meteosat Second Generation (MSG) 10.8 μm image (in normalized inverted greyscale). VMI values above 45 dBZ are associated with intense precipitation which occurred during convective events. The zoom over the CI target area shows a line of convective cells along the Apennines in central Italy due to the western flow approaching the orographic barrier.

## 2.2 WRF model set up

The numerical weather prediction experiments are performed in this work using the non hydrostatic Advanced Research WRF (ARW) modeling system V3.4.1. It is a primitive equations mesoscale meteorological model, with terrain-following vertical coordinates and options for different physical parameterizations. Skamarock et al. (2008) provides a detailed overview of the model.

In this study, a one-way nested configuration using *ndown* program is used: a 12km domain (263x185) that covers central Europe and west Mediterranean basin (referred as D01) is initialized using the ECMWF analyses at 0.25 degrees of horizontal resolution; an innermost domain, that covers the whole Italy (referred as D02), with a grid space of 3km (445x449) using as BC and IC the output of the previous forecast at 12km. Both domains run with 37 unequally spaced vertical levels, from the surface up to 100 hPa (Figure 5).

Taking into account that the performance of a mesoscale model is highly related to the parameterization schemes, the main physics packages used in this study are set as for the operational configuration (Ferretti et al., 2014) used at the centre of Excellence CETEMPS, which include (Skamarock et al., 2008): the "New" Thompson et al. 2004 microphysics scheme, the MYJ (Mellor-Yamada-Janjic) scheme for the PBL (planetary boundary layer), the Goddard shortwave radiation scheme and the RRTM (rapid radiative transfer model) longwave radiation scheme, the Eta similarity scheme for surface layer formulation and the Noah LSM (Land Surface Model) to parameterize physics of land surface. A few preliminary tests are performed to assess the best cumulus parameterization scheme to be used both for the coarse and finest resolution domain for this event. Hence the following parameterizations are tested: the new Kain–Fritsch and the Grell 3D schemes. The latter is an enhanced version of the Grell-Deveneyi scheme, in our simulations only used on the lowest resolution domain, where the option *cugd_avedx* (subsidence spreading) is switched on. Based on the results of these two cumulus parameterization schemes, the one producing the best precipitation forecast will be used to evaluate the impact of data assimilation.

# 3 Data and methodology

This section will be focused on the description of types of observations ingested into the assimilation procedure, both conventional and not conventional, and on the 3D-Var methodology and the observation operator used for the calculation of the reflectivity.

### 3.1 Observations to be assimilated

Conventional observations SYNOP and TEMP were retrieved from the European Centre for Medium-Range Weather Forecasts (ECMWF) Meteorological Archival and Retrieval System (MARS). They have been converted from BUFR to LITTLE_R format before to be assimilated into the 3D-Var system. A total of 989 observations (967 SYNOP and 22 TEMP) are ingested into the coarse resolution domain, whereas a total of 338 (331 SYNOP and 7 TEMP) observations into the high resolution one.

Volumetric reflectivity taken from three C-band Doppler radars operational during the IOP4 have been assimilated to improve IC. Radars have different technical characteristics and were operated with different scanning strategies and operational settings as shown in Table 1.

Monte Midia (MM) and San Pietro Capofiume (SPC) radars are included in the Italian radar network, while Polar 55C (P55C) radar is a research radar working on demand which was operational during HyMeX IOPs (Roberto et al., 2016). Radar data can be affected by numerous sources of errors, mainly due to ground clutter, attenuation due to propagation or beam blocking, anomalous propagation and radio interferences. This is the reason why a preceding "cleaning" procedure is applied to the acquired radar reflectivity from the three radars before the assimilation process, consisting of the following 2 steps:

- pre-processing consists of a first quality check of radar volumes where radar pixel affected by ground clutter and anomalous propagation were filtered. Furthermore, Z was corrected for attenuation using a methodology based on the specific differential phase shift ($K_{dp}$) available for dual polarization radars (Vulpiani et al, 2015);
- conversion to the model format is applied to all radars reflectivity data: an ad hoc shell script in Fortran language has been written and adapted to each radar characteristics.

### 3.2 3D-Var data assimilation method

Data assimilation (DA), which applications arise in many fields of geosciences perhaps most importantly in weather forecasting and hydrology, in this context is the procedure by which observations are combined with the product (*first guess* or *background forecast*) of a NWP model and their corresponding error statistics to produce a bettered estimate (the *analysis*) of the true state of the atmosphere (Skamarock et al., 2008). The variational DA method realizes this through the iterative minimization of a penalty function (Ide et al., 1997):

$$J(\boldsymbol{x}) = J^b(\boldsymbol{x}) + J^0(\boldsymbol{x}) = \frac{1}{2}\{[\boldsymbol{y}^0 - H(\boldsymbol{x})]^T \boldsymbol{R}^{-1}[\boldsymbol{y}^0 - H(\boldsymbol{x})] + (\boldsymbol{x} - \boldsymbol{x}^b)^T \boldsymbol{B}^{-1}(\boldsymbol{x} - \boldsymbol{x}^b)\}, \quad (1)$$

where $\boldsymbol{x}^b$ is the first guess state vector, $\boldsymbol{y}^0$ is the assimilated observation vector, $H$ is the observation operator that links the model variables to the observation variables and $\boldsymbol{x}$ is the unknown analysis state vector to be found by minimizing

$J(\boldsymbol{x})$. Finally $\boldsymbol{B}$ and $\boldsymbol{R}$ are the background covariance error matrix and the observation covariance error matrix, respectively.

The minimization of the penalty function $J(\boldsymbol{x})$, displayed by Equation (1), is the a posteriori maximum likelihood estimate of the true atmosphere state, given the two sources of a priori data that are $\boldsymbol{x}^b$ and $\boldsymbol{y}^0$ (Lorenc, 1986).

In this study the 3D-Var system developed by Barker et al. (2003, 2004) is used for assimilating radar reflectivity and conventional observations SYNOP and TEMP. The penalty function minimization is performed in a preconditioned control variable space, where the preconditioned control variables are pseudo relative humidity, stream function, unbalanced temperature, unbalanced potential velocity and unbalanced surface pressure. Because of radar reflectivity assimilation is considered, the total water mixing ratio $q_t$ is chosen as the moisture control variable. The following Equation (2) presents the observation operator used by the 3D-Var to calculate reflectivity for the comparison with the observed one (Sun and Crook, 1997):

$$Z = 43.1 + 17.5\, log(\rho q_r), \tag{2}$$

where $\rho$ and $q_r$ are the air density in kg/m$^3$ and the rainwater mixing ratio in g/kg, respectively, while $Z$ is the co-polar radar reflectivity factor expressed in dBZ. Since the total water mixing ratio $q_t$ is used as the control variable, a warm rain process (Dudhia, 1989) is introduced into the WRF-3D-Var system: this allowed for producing the increments of moist variables linked to the hydrometeors.

The performance of the DA system strongly depends on the quality of the $\boldsymbol{B}$ matrix in Equation (1). In this study, a specific background error statistics is computed for both domains using the National Meteorological Center (NMC) method (Parrish and Derber, 1992). To evaluate the NMC-based error statistics, the differences between two forecasts at t+24 and t+12 (performed every day and valid at the same time), are used to calculate the domain-averaged error statistics for the entire SOP1 period (5 September - 5 November 2012). T+24 minus T+12 is typical for regional applications; it is important to include forecast differences to remove the diurnal cycle.

## 4 Design of the numerical experiments: discussion of the results

The simulations on the coarser resolution domain (D01) are run from 12:00UTC of 13 September 2012 and integrated for the following 96 hours, whereas runs on the finest resolution domain started at 00:00UTC of September 14 for a total of 48 hours of integration. The previous coarser resolution WRF forecast at 00:00UTC is used as the first guess (FG) in the 3D-Var experiment, because 00:00UTC has been selected as the "*analysis time*" of the assimilation procedure. After assimilation, the lateral and lower boundary conditions are updated for the high resolution forecast. Finally, the new IC and BC are used for the model initialization (in a warm start regime) at 00:00UTC. As already pointed out a set of preliminary experiments are performed using different cumulus convective scheme to assess the best one to be used. The following experiments are performed without assimilation and using the convective scheme on the coarser resolution domain only: KAIN-FRITSCH (KF_MYJ); GRELL3D (GRELL3D_MYJ); GRELL3D associated with the CUGD factor (GRELL3D_MYJ_CUGD). A summary of these numerical experiments is given in Table 2.

The analysis of the results of these set of experiments allows establishing the best model configuration for the radar reflectivity assimilation experiments. The DA experiments aim to investigate:

1. the impact of the assimilation at low and high resolution by assimilating both conventional and non-conventional data at both resolutions;
2. the impact of the assimilation of different types of observations;
3. the impact of the different radars, which is investigated by performing experiment by assimilating conventional data and then adding radar one by one.

The following experiments, summarized in Table 3, are performed: i) the control simulation (CTL) without data assimilation; the assimilation of conventional (SYNOP and TEMP) data only (CON); ii) the assimilation of reflectivity data from MM only (CONMM) are added; iii) the assimilation of P55C radar reflectivity is added to the previous experiments (CONMMPOL); iv) the assimilation of the third radar reflectivity data is added to the previous (CONMMPOLSPC). Finally, an experiment to assess the role of the outer loop is performed (CONMMPOLSPC3OL). To include non-linearity into the observation operator and to evaluate the impact of reflectivity data entering for each cycle, the multiple outer loops strategy is applied (Rizvi et al., 2008). According to this approach, the non-linear problem is solved iteratively as a progression of linear problems: the assimilation system is able to ingest more observations by running more than one analysis outer loop.

The MET (Model Evaluation Tools) application (DTC, 2013), developed at the DTC (Developmental Testbed Center, NCAR), has been used to objectively evaluate the 12 hours accumulated precipitation produced by WRF on the high resolution domain. The observations used for the statistical evaluation were obtained from the DEWETRA platform of the Department of Civil Protection and the comparison has been performed over central Italy target area using about 3000 rain gauges with a good coverage throughout the area.
In this section the results will be presented and discussed following the rationale of the previously introduced experiments and using statistical indexes for performance quantitative assessment.

### 4.1 Sensitivity test to cumulus parameterization

From the sensitivity test to different cumulus parameterization scheme (Table 2) the best performance is obtained by Grell3D scheme which is able to simulate the peak precipitation cumulated in 24 hours over Campo Imperatore, whereas KAIN-FRITSCH completely misses it (not shown here). The MET statistical analysis support the previous finding and the simulation with *cugd_avedx* activated shows higher performances in terms of accuracy, equitable threat score and false alarm ratio than the other two simulations. Here after GRELL3D_MYJ_CUGD is referred as the control experiment (CTL) performed without any data assimilation. Therefore, a new set of simulations are performed following the previous strategies already mentioned in Section 4.

### 4.2 Impact of conventional and radar reflectivity assimilation on rainfall forecast: low versus high resolution

In figure 6 a preliminary comparison among low resolution (LR) simulations is shown. The control simulation (CTL) without data assimilation is shown in Figure 6a; whereas the other panels (b, c, d, e) show the experiments performed using the data assimilation.

Observing the outputs of different experiments (Fig. 6) listed in Table 3, best simulation is found for CONMMPOLSPC_LR_12KM (black arrow in Fig.6e): the rainfall maximum over Campo Imperatore is very well simulated, however a cell displacement at the border between Marche and Abruzzo regions is noticeable. Furthermore the precipitation feature along the coasts (black oval) is also forecasted.

The statistical indices (Fig. 7) quite support this finding: for example the brown curve (CONMMPOLSPC_LR_12KM) produced the best ACC and FAR for thresholds lower than 20mm/12h, whereas quite good values are found for ETS for thresholds between approximately 3 and 15mm/12h.

Similarly to the above comparison, high resolution results (HR) are presented in figure 8 obtained performing reflectivity assimilation only on 12km domain (column 1), only on 3km (column 2) and both on 12km and 3km (column 3); to the top of figure 8 the CTL experiment on D02 is shown. Figure 8 is organized as follows: viewing panels by line, on line 1 all the simulations with conventional data assimilation only (CON*) are found; on line 2 all the experiments with the assimilation of the reflectivity data from MM radar added (CONMM*); on line 3 all the experiments with the assimilation of the reflectivity data from 2 C-band radars added (CONMMPOL*); on line 4 all the experiments with the assimilation of the reflectivity data from all 3 C-band radars added (CONMMPOLSPC*); on line 5 the simulations where the strategy of outer loop is adopted (CONMMPOLSPC3OL*). For these experiments the values of the main statistical indices (ACC, FBIAS, ETS, FAR) have been summarized over tables reporting only two thresholds of precipitation: 1 mm/12h and 20 mm/12h (light and heavy rain regimes).

In order to investigate the impact of the assimilation at different resolutions, we analyze figure 8 by column and comparing it with the observation (Fig. 2); the statistical analysis is also used:

- column 1 (12KM): CTL produces an overestimation of the rainfall that is not corrected by the assimilation of conventional data, but assimilating the reflectivity from the 3 radars and introducing the 3 outer loops (Fig. 8 column 1 line 4) the main cells are better reproduced. MET indices in Table 4 suggest that CTL and CONMMPOLSPC3OL_HR_12KM are the simulations with the best response, secondly CONMM_HR_12KM;
- column 2 (3KM): a partial correction of the rainfall overestimation compared to column 1 is observed especially if reflectivity from all the radars are assimilated and the outer loop strategy is applied; the statistical indices in Table 5 show CONMMPOLSPC3OL_3KM as the best experiment among the assimilated ones;
- column 3 (12KM_3KM): rainfall overestimation was partially corrected compared to columns 1 and 2 by all experiments; the MET statistics in Table 6 shows that CTL and CONMMPOLSPC3OL_12KM_3KM are the experiments that return better values.

Summarizing, the previous analysis suggests that the frequency of rainfall overestimation for higher thresholds has been reduced by radar reflectivity assimilation performed only on D01. Furthermore, improvements come out for heavy rain regimes when radar reflectivity assimilation has been performed on the highest resolution domain, whereas the ingestion of conventional observations produces the worst results since a smaller number of them were assimilated into the finest resolution domain than that the coarser one. The assimilation, operated on both 12km and 3km, gives better results than the ones on column 1, but a worse response than the others on column 2 is given for higher thresholds.

In order to examine the impact of the assimilation of different data and radars, we can now analyze the experiments showed in figure 8 by line. The results are compared with the observations of Fig. 2. The following considerations are worth discussing:

- line 1 (CON): a strong reduction of the rainfall is found with respect to CTL if conventional data are assimilated, but the rainfall pattern remains unchanged; statistical indices in Table 7 seem do not improve performances of CTL. The indices values suggest a slightly better performance when the conventional observations are assimilated only on the bigger domain;
- line 2 (CONMM): a further reduction in the precipitation overestimation is found as well as some variations in the pattern of the rainfall; statistics in Table 8 shows that MM radar reflectivity assimilation improves model performance above all for higher thresholds; conventional observations assimilation in tandem with MM gives better results;
- line 3 (CONMMPOL): a quite strong improvement in the rainfall amount is found for all simulations. From the statistics of Table 9 we have found a worsening of the results especially for heavy rain regimes when POL is added (FBIAS and ETS); a better answer is given by the simulation where assimilation is performed on both domains;
- line 4 (CONMMPOLSPC): a clear correction of the rainfall pattern is found; the overestimation produced by the simulation where the reflectivity from all the radars are assimilated on the 3km domain has been corrected by the experiment in which the reflectivity is assimilated both on D01 and D02; statistical indices in Table 10 suggest that the addition of SPC radar improves the results, furthermore they are not better than those where only MM is ingested;
- line 5 (CONMMPOLSPC3OL): the outer loop experiment confirms the overestimation reduction by *12KM_3KM; from Table 11 it seems that the introduction of 3OL improves the indices values above all when the 12km domain is considered; CONMMPOLSPC3OL_12KM_3KM can be considered the best simulation.

In summary, simulations results show that assimilation of conventional data is better to perform on the lowest resolution domain because more observations were used in the coarser domain, whereas when the assimilation is performed on the highest resolution domain only few SYNOP and even less TEMP fell down in the 3km domain at the analysis time of the assimilation procedure. With regard to the assimilation of reflectivity radar data, due to its location Apennines range screen radar beam and POL underestimates rainfall where the peak precipitation occurs, passing to the model wrong estimates thus worsening assimilation results. Also the outer loop strategy could have an important role in the assimilation procedure, but this latter needs a further investigation because a general rainfall underestimation for higher thresholds is found.

## 5 Conclusions

In this manuscript the effects of multiple radar reflectivity data assimilation on a heavy precipitation event occurred during the SOP1 of the HyMeX campaign have been evaluated: the aim is to build a regionally-tuned numerical prediction model and decision-support system for civil prevention and protection within the central Italian regions. A

sensitivity study at different domain resolution and using different types of data to improve initial conditions has been performed by assimilating into the WRF model radar reflectivity measurements, collected by three C-band Doppler weather radars operational during the event that hit central Italy on 14 September 2012. The 3D-Var and MET are the WRF tools used to assess this purpose. First of all, WRF model responses to different types of cumulus parameterizations have been tested to establish the best configuration and to obtain the control simulation. The latter has been compared with observations and other experiments performed using 3D-Var. The set of assimilation experiments have been conducted following two different strategies: i) data assimilation at low and high resolution or at both resolutions simultaneously; ii) conventional data against radar reflectivity data assimilation. Both have been examined to assess the impact on rainfall forecast.

The major findings of this work have been the following:

- Grell 3D parameterization improves the simulations both on D01and D02 and the use of the spreading factor is an added value in properly predict heavy rainfall over inland of Abruzzo and the rainfall pattern along the northeast coast;
- investigating the impact of the assimilation at different resolutions, best results are showed by the experiments where the data assimilation is performed on both domains 12km and 3km;
- the impact of the assimilation using different types of observations shows improvements if reflectivity from all the radars together with SYNOP and TEMP are assimilated; furthermore MM is the one that better impact the model results because of it has been better detected the event;
- the outer loop strategy allows for further improving positive impact of the assimilation of multiple reflectivity radars data. Moreover, a deeper investigation of multiple outer loops strategy is required to assess its impact.

Analyzing the results obtained in this study, it is not possible to assess which is, in general, the best model configuration since this analysis should be performed systematically with a significant number of flash flood case studies. However, this work was an interesting study in 3D-Var reflectivity data assimilation that can encourage to investigate more flash flood cases occurred over central Italy, in order to make this proposed approach suitable to provide a realistic prediction of possible flash floods both for the timing and localization of such events. To confirm and consolidate these initial findings, apart from analyzing more case studies, a deeper analysis of the meteorology of the region and of the performance of the data assimilation system throughout longer trials in a "pseudo-operational" procedure is necessary.

**Acknowledgements**

We are grateful to the Gran Sasso National Laboratories for support in computing resources, as well as the National Civil Protection Department and CIMA Research Foundation for rain gauges data using for the model validation. NCAR is also acknowledge for WRF model, 3D-Var system and MET tool. This work aims at contributing to the HyMeX programme.

**References**

370 Barker, D.M., Huang, W., Guo, Y.-G., and Bourgeois, A.: A Three-Dimensional Variational (3D-Var) Data
371 Assimilation System For Use With MM5. NCAR Tech. Note, NCAR/TN-453+STR, UCAR Communications, Boulder,
372 CO, 68pp, 2003.

373 Barker, D.M., Huang, W., Guo, Y.-R., Bourgeois, A., and Xiao, Q.: A Three-Dimensional Variational (3D-Var) Data
374 Assimilation System For Use With MM5: Implementation and Initial Results. *Mon. Wea. Rev*., 132, 897-914, 2004.

375 Daley, R.: Atmospheric Data Analysis, Cambridge University Press, Cambridge, UK, 1991.

376 Das, M. K., M. A. M. Chowdhury, S. Das, S. K. Debsarma, and S. Karmakar: Assimilation of Doppler weather radar
377 data and their impacts on the simulation of squall events during premonsoon season. Natural Hazards, 77(2), 901–931.
378 DOI: 10.1007/s11069-015-1634-9, 2015.

379 Davolio, S., Ferretti, R., Baldini, L., Casaioli, M., Cimini, D., Ferrario, M. E., Gentile, S., Loglisci, N., Maiello, I.,
380 Manzato, A., Mariani, S., Marsigli, C., Marzano, F. S., Miglietta, M. M., Montani, A., Panegrossi, G., Pasi, F., Pichelli,
381 E., Pucillo, A. and Zinzi, A.: The role of the Italian scientific community in the first HyMeX SOP: an outstanding
382 multidisciplinary experience. *Meteorologische Zeitschrift*, 24, 261-267, 2015.

383 Developmental Testbed Center, 2013: MET: Version 4.1 Model Evaluation Tools Users Guide. Available at
384 http://www.dtcenter.org/met/users/docs/overview.php. 226 pp.

385 Diodato N. and Bellocchi G. (eds.), Storminess and Environmental Change, Advances in Natural and Technological
386 Hazards Research 39, DOI 10.1007/978-94-007-7948-8_2, *Springer Science+Business Media Dordrecht* 2014.

387 Dixon, M., Li, Z., Lean, H., Roberts, N., and Ballard, S.: Impact of data assimilation on forecasting convection over the
388 United Kingdom using a high-resolution version of the Met Office Unified Model, Mon. Weather Rev., 137, 1562–
389 1584, 2009.

390 Ducrocq, V., Braud, I., Davolio, S., Ferretti, R., Flamant, C., Jansà, A., Kalthoff, N., Richard, E., Taupier-Letage, I.,
391 Ayral, P.-A., Belamari, S., Berne, A., Borga, M., Boudevillain, B., Bock, O., Boichard, J.-L., Bouin, M.-N., Bousquet,
392 O., Bouvier, C., Chiggiato, J., Cimini, D., Corsmeier, U., Coppola, L., Cocquerez, P., Defer, E., Delanoë, J., Di
393 Girolamo, P., Doerenbecher, A., Drobinski, P., Dufournet, Y., Fourrié, N., Gourley, J. J., Labatut, L., Lambert, D., Le
394 Coz, J., Marzano, F. S., Molinié, G., Montani, A., Nord, G., Nuret, M., Ramage, K., Rison, B., Roussot, O., Said, F.,
395 Schwarzenboeck, A., Testor, P., Van-Baelen, J., Vincendon, B., Aran, M. and Tamayo, J.,: HyMeX-SOP1, the field
396 campaign dedicated to heavy precipitation and flash flooding in the northwestern Mediterranean. *Bulletin of the*
397 *American Meteorological Society*, **95**, 1083-1100, 2014.

398 Dudhia, J.: Numerical study of convection observed during the winter monsoon experiment using a mesoscale two-
399 dimensional model, J. Atmos. Sci., 46, 3077–3107, 1989.

400 Ferretti, R., E. Pichelli, S. Gentile, I. Maiello, D. Cimini, S. Davolio, M. M. Miglietta, G. Panegrossi, L. Baldini, F.
401 Pasi, F. S. Marzano, A. Zinzi, S.Mariani, M. Casaioli, G. Bartolini, N. Loglisci, A. Montani, C. Marsigli,A.Manzato, A.
402 Pucillo, M. E. Ferrario, V. Colaiuda, and R. Rotunno: Overview of the first HyMeX Special Observation Period over
403 Italy: observations and model results. Hydr. Earth Syst. Sci., 18, 1953-1977,2014, doi:10.5194/hess-18-1953-2014,
404 2014.

Ha, J.-H., H.-W. Kim, and D.-K. Lee: Observation and numerical simulations with radar and surface data assimilation for heavy rainfall over central Korea. Advances in Atmospheric Sciences, 28(3), 573–590. DOI: 10.1007/s00376-0100035-y, 2011.

Hertig E., Paxian A., Vogt G., Seubert S., Paeth H., Jacobeit J.: Statistical and dynamical downscaling assessments of precipitation extremes in the Mediterranean area. *Meteorologische Zeitschrift*, Vol. 21 No. 1 , p. 61 - 77, 2012.

Ide, K., Courtier, P., Ghil, M., and Lorenc, A. C.: Unified notation for data assimilation: Operational, sequential and variational, J. Meteorol. Soc. Jpn., 75, 181–189, 1997.

Italian Civil Protection Department and CIMA Research Foundation: The Dewetra Platform: A Multi-perspective Architecture for Risk Management during Emergencies. Springer International Publishing Switzerland, Chapter Information Systems for Crisis Response and Management in Mediterranean Countries, Volume 196 of the series Lecture Notes in Business Information Processing pp 165-177, 2014. DOI 10.1007/978-3-319-11818-5_15

Llasat, M. C., Llasat-Botija, M., Petrucci, O., Pasqua, A. A., Rosselló, J., Vinet, F., and Boissier, L.: Towards a database on societal impact of Mediterranean floods within the framework of the HYMEX project, Nat. Hazards Earth Syst. Sci., 13, 1337-1350, doi:10.5194/nhess-13-1337-2013, 2013.

Lee, J.-H., H.-H. Lee, Y. Choi, H.-W. Kim, and D.-K. Lee: Radar data assimilation for the simulation of mesoscale convective systems. Advances in Atmospheric Sciences, 27(5), 1025–1042. DOI: 10.1007/s00376-010-9162-8, 2010.

Liu, J., M. Bray, and D. Han: A study on WRF radar data assimilation for hydrological rainfall prediction. Hydrology and Earth System Sciences, 17(8), 3095– 3110. DOI: 10.5194/hess-17-3095-2013, 2013.

Lorenc, A. C.: Analysis methods for numerical weather prediction, Q. J. Roy. Meteorol. Soc., 112, 1177–1194, 1986.

Maiello, I., Ferretti, R., Gentile, S., Montopoli, M., Picciotti, E., Marzano, F. S., and Faccani, C.: Impact of radar data assimilation for the simulation of a heavy rainfall case in central Italy using WRF–3DVAR, Atmos. Meas. Tech., 7, 2919-2935, doi:10.5194/amt-7-2919-2014, 2014.

Martín J. R., García M. M., Dávila F. de P., Soriano L. R.: Severe rainfall events over the western Mediterranean Sea: A case study. *Atmospheric Research*, 127, 47–63, 2013.

Nakatani T., Misumi R., Shoji Y., Saito K., Seko H., Seino N., Suzuki S-I.,Shusse Y., Maesaka T., and Sugawara H. ; Tokyo metropolitan area convection study for extreme weather resilient cities. *BAMS*, 96, ES123-ES126, 2015.

Parrish, D.F. and Derber, J.C.: The National Meteorological Center's Spectral Statistical-Interpolation Analysis System. *Mon. Wea. Rev.*, 120, 1747-1763, 1992.

Rizvi, S., Guo, Y.-R, Shao, H., Demirtas, M., and Huang, X.-Y.: Impact of outer loop for WRF data assimilation system (WRFDA). 9th WRF Users' Workshop, Boulder, Colorado, 23-27 June 2008.

Roberto, N., Adirosi, E., Baldini, L., Casella, D., Dietrich, S., Gatlin, P., Panegrossi, G., Petracca, M., Sanò, P., and Tokay, A.: Multi-sensor analysis of convective activity in central Italy during the HyMeX SOP 1.1, Atmos. Meas. Tech., 9, 535-552, doi:10.5194/amt-9-535-2016, 2016.

Salonen K, Haase G, Eresmaa R, Hohti H, Järvinen H.: Towards the operational use of Doppler Radar radial winds in HIRLAM. Atmospheric Research 100: 190–200, 2010.

Skamarock, W.C., Klemp, J.B., Dudhia, J., Gill, D.O., Barker, D.M., Duda, M. G., Huang, X.-Y., Wang, W., and Powers, J. G.: A description of the Advanced Reasearch WRF Version 3. NCAR Technical Note. TN 475+STR, 113 pp., available from www.mmm.ucar.edu/wrf/users/docs/arw_v3.pdf (last access: January 2012), 2008.

Sokol, Z. and Rezacova, D.: Assimilation of Radar reflectivity into the LMCOSMO model with a high horizontal resolution, Meteorol. Appl., 13, 317–330, 2006.

Sokol, Z.: Effects of an assimilation of Radar and satellite data on a very short range forecast of heavy convective rainfalls, Atmos. Res., 93, 188–206, 2009.

Stanesic A., and K.A. Brewester: Impact of Radar Data Assimilation on the Numerical Simulation of a Severe Storm in Croatia. Met.Zeit. Vol. 25, No. 1, 37–53, 2016

Sugimoto, S., Crook N.A., Sun J., Xiao Q., and Barker D.M.: An examination of WRF 3D-VarRadar data assimilation on its capability in retrieving unobserved variables and forecasting precipitation through observing system simulation experiments. *Mon. Wea. Rev.*, 137, 4011-4029, 2009. DOI:10.1175/2009MWR2839.1.

Sun, J. Xue, M., Wilson J. W., Zawadzki I., Ballard S.P., Onvlee-Hooimeyer J., Joe P., Barker D.M., Li P-W., Golding B., Xu M., and Pinto J.: Use of NWP for nowcasting convective precipitation, recent progress and challenges. *BAMS*, 95, 409-426, 2014.

Sun, J. and Crook, N.A.: Dynamical and Microphysical Retrieval from Doppler RADAR Observations Using a Cloud Model and Its Adjoint. Part I: Model Development and Simulated Data Experiments. *J. Atmos. Sci.*, 54, 1642-1661, 1997.

Thompson, G., R. M. Rasmussen, and K. Manning: Explicit forecasts of winter precipitation using an improved bulk microphysics scheme. Part I: Description and sensitivity analysis. Mon. Wea. Rev.,132, 519–542, 2004.

Vulpiani G., Pagliara, P., Negri, M., Rossi, L., Gioia, A., Giordano, P., Alberoni, P. P., Cremonini, R., Ferraris, L., and Marzano, F. S.: The Italian radar network within the national early-warning system for multi-risks management, Proc. of Fifth European Conference on Radar in Meteorology and Hydrology (ERAD 2008), 184, Finnish Meteorological Institute, Helsinki, 30 June-4 July, 2008a.

Vulpiani, G., Baldini, L., and Roberto, N.: Characterization of Mediterranean hail-bearing storms using an operational polarimetric X-band radar, Atmos. Meas. Tech., 8, 4681-4698, doi:10.5194/amt-8-4681-2015, 2015.

Xiao, Q., Kuo, Y.-H., Sun, J. and Lee, W.-C.: Assimilation of Doppler RADAR Observations with a Regional 3D-Var System: Impact of Doppler Velocities on Forecasts of a Heavy Rainfall Case. *J. Appl. Meteor.*,44, 768-788, 2005.

Xiao, Q. and Sun, J.: Multiple-RADAR Data Assimilation and Short-Range Quantitative Precipitation Forecasting of a Squall Line Observed during IHOP_2002. *Mon. Wea. Rev.*, 135, 3381-3404, 2007.

## LIST OF FIGURES

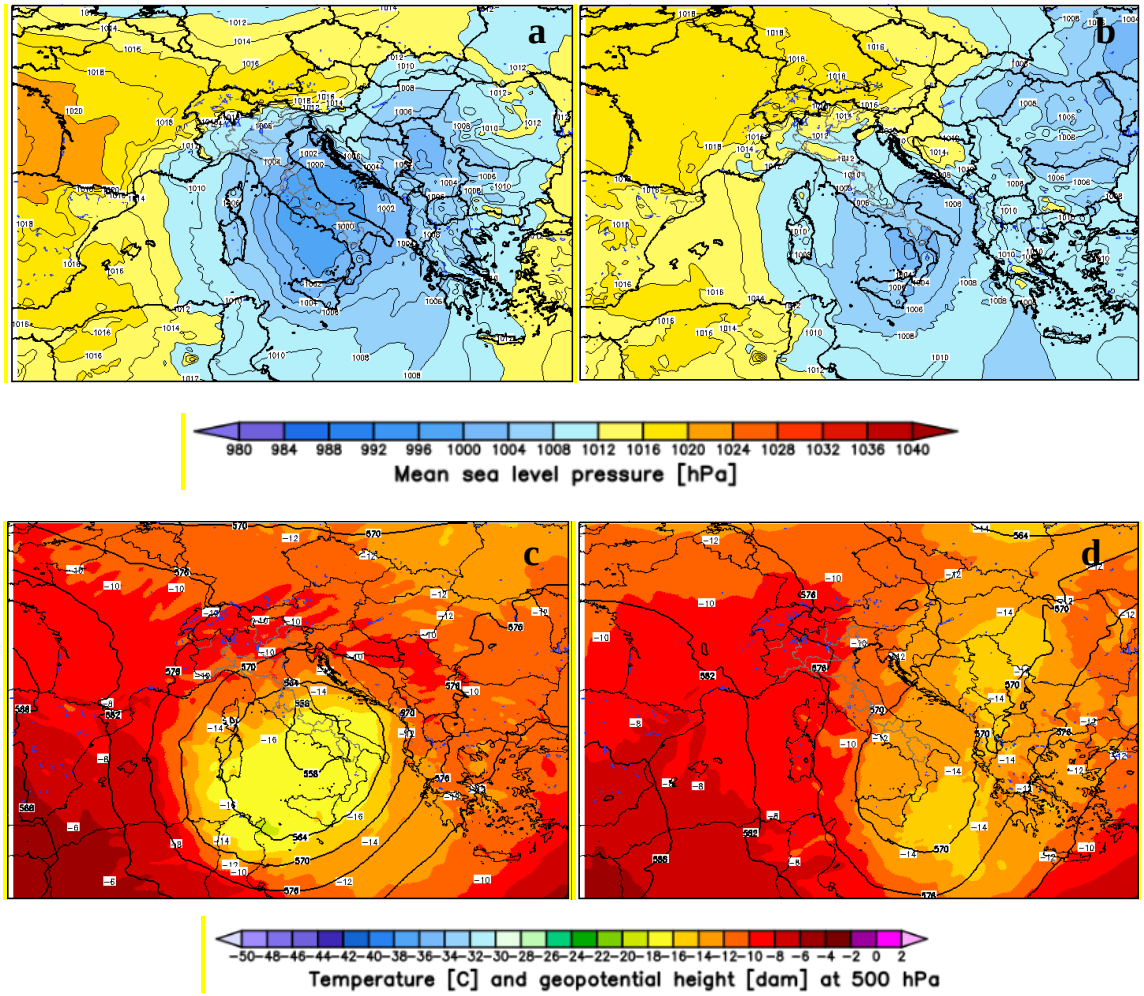


**Figure 1: Mean sea level pressure (a, b), temperature (black isolines) and geopotential height (color shades) at 500 hPa (c, d) at 12:00UTC on 14 September and 15 September 2012, respectively**

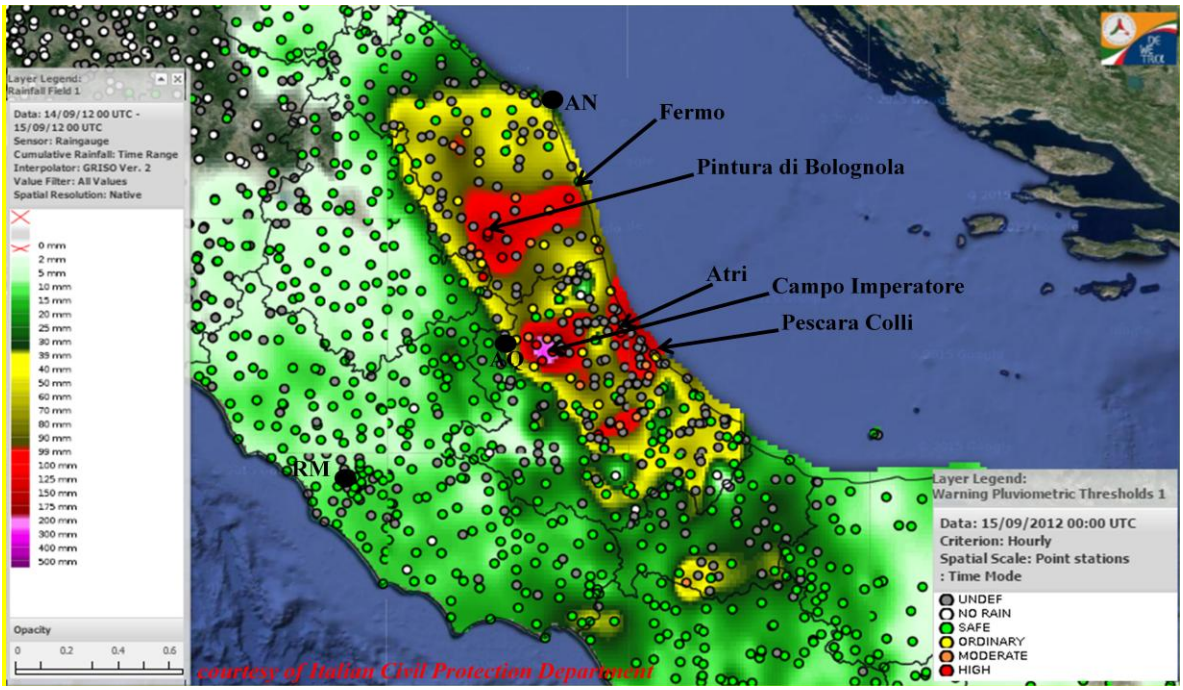


**Figure 2: Interpolated map of 24h accumulated rainfall from 00:00UTC of 14 September 2012 over Abruzzo and Marche regions from DEWETRA system obtained by rain gauges measurements. Black contours are the administrative boundaries of Regions, while the colored circles represent the warning pluviometric thresholds.**

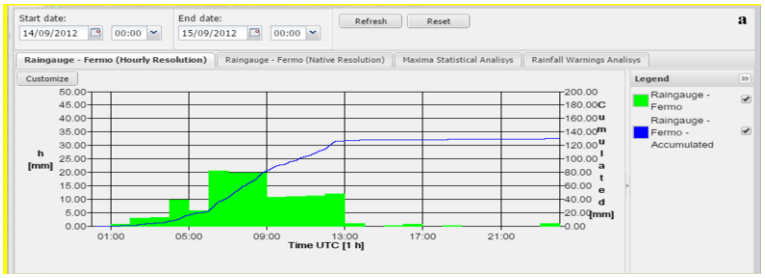


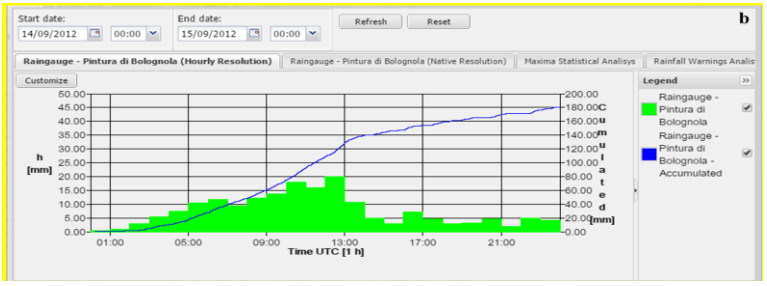


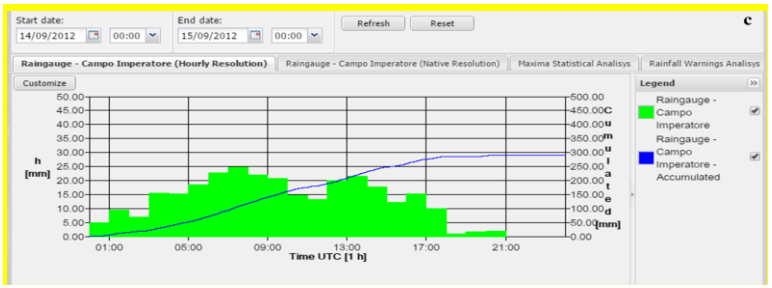

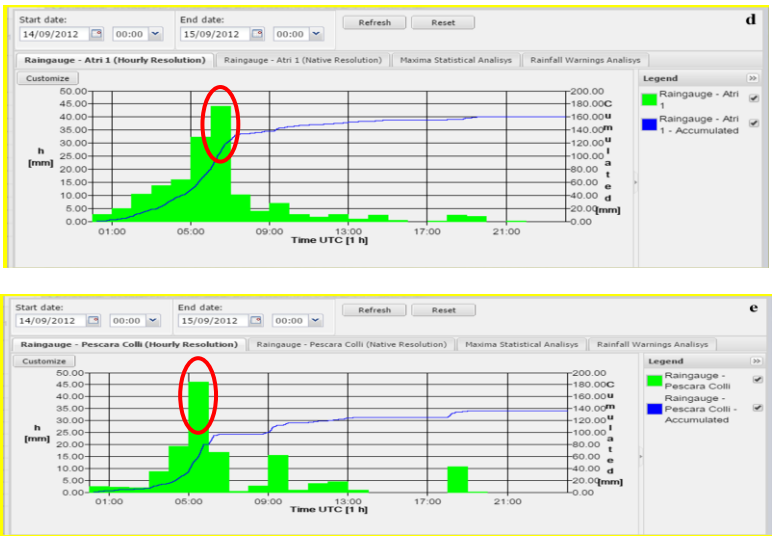


**Figure 3: Rain gauges time series of some selected stations in Marche (a and b) and Abruzzo (c, d and e) regions during the event of 14 September 2012. The green histogram represents the hourly accumulated precipitation (scale on the left); the blue line represents the incremental accumulation within the 24h (scale on the right). (*courtesy of Italian Civil Protection Department*)**

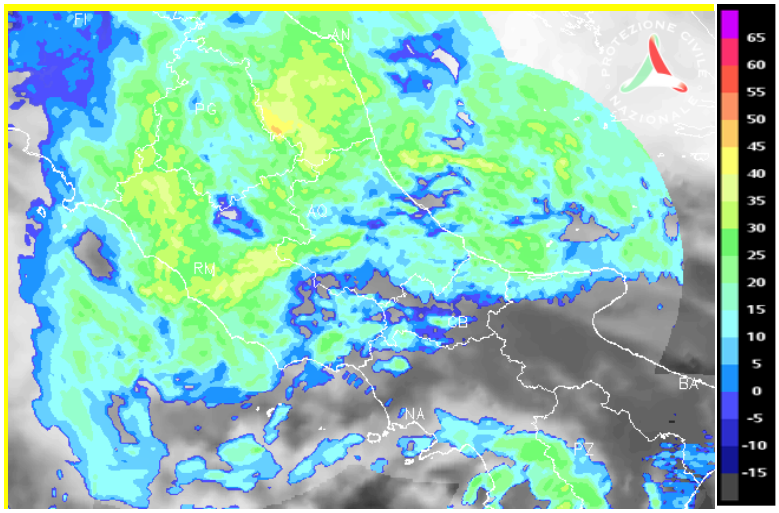


**Figure 4: Zoom over CI of the VMI on 14September 2012 at 08:00UTC from the Italian radar network overlapped with the MSG (IR 10.8) at 07:30UTC. (*courtesy of Italian DPC*)**

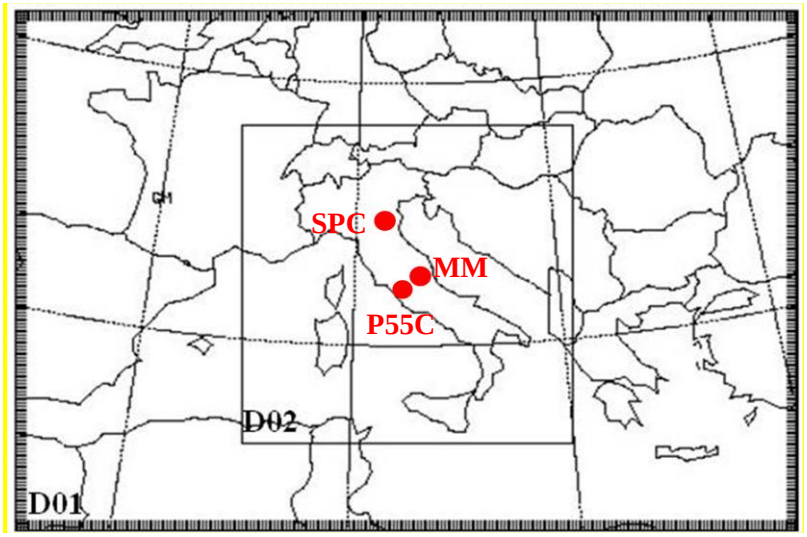


**Figure 5: WRF *ndown* domains configuration: the two domains have respectively resolution of 12km and 3km. The high resolution D02 over Italy includes Mt. Midia (MM), ISAC-CNR (P55C) and San Pietro Capofiume (SPC) radars (red dots in the figure).**

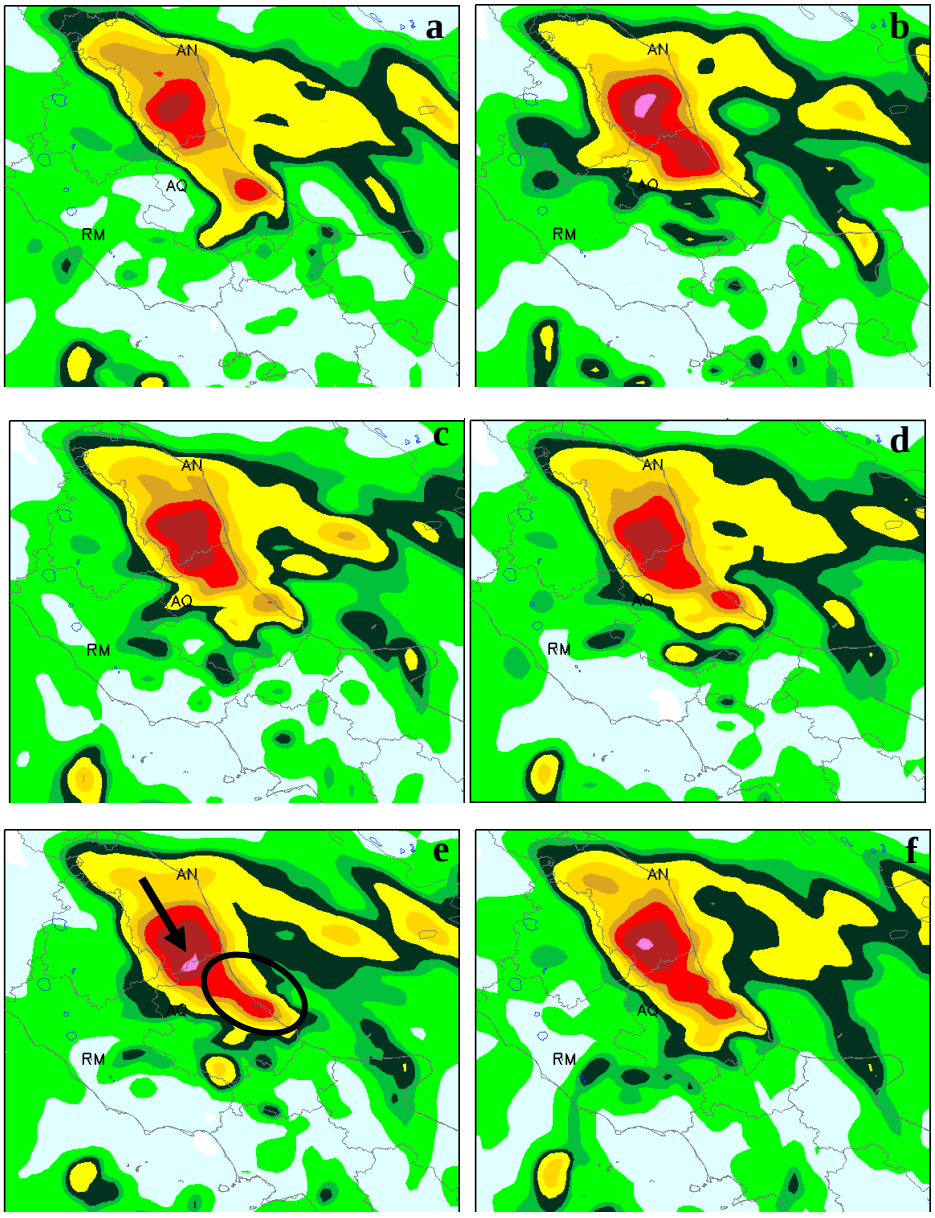

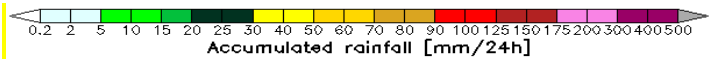


**Figure 6: WRF D01 accumulated 24h rainfall forecast over central Italy from 00:00UTC of 14 September 2012: a) WRF D01 CTL; b) WRF D01 CON_LR_12KM; c) WRF D01 CONMM_LR_12KM;d)WRF D01 CONMMPOL_LR_12KM; e) WRF D01 CONMMPOLSPC_LR_12KM; f) WRF D01 CONMMPOLSPC3OL_LR_12KM.**

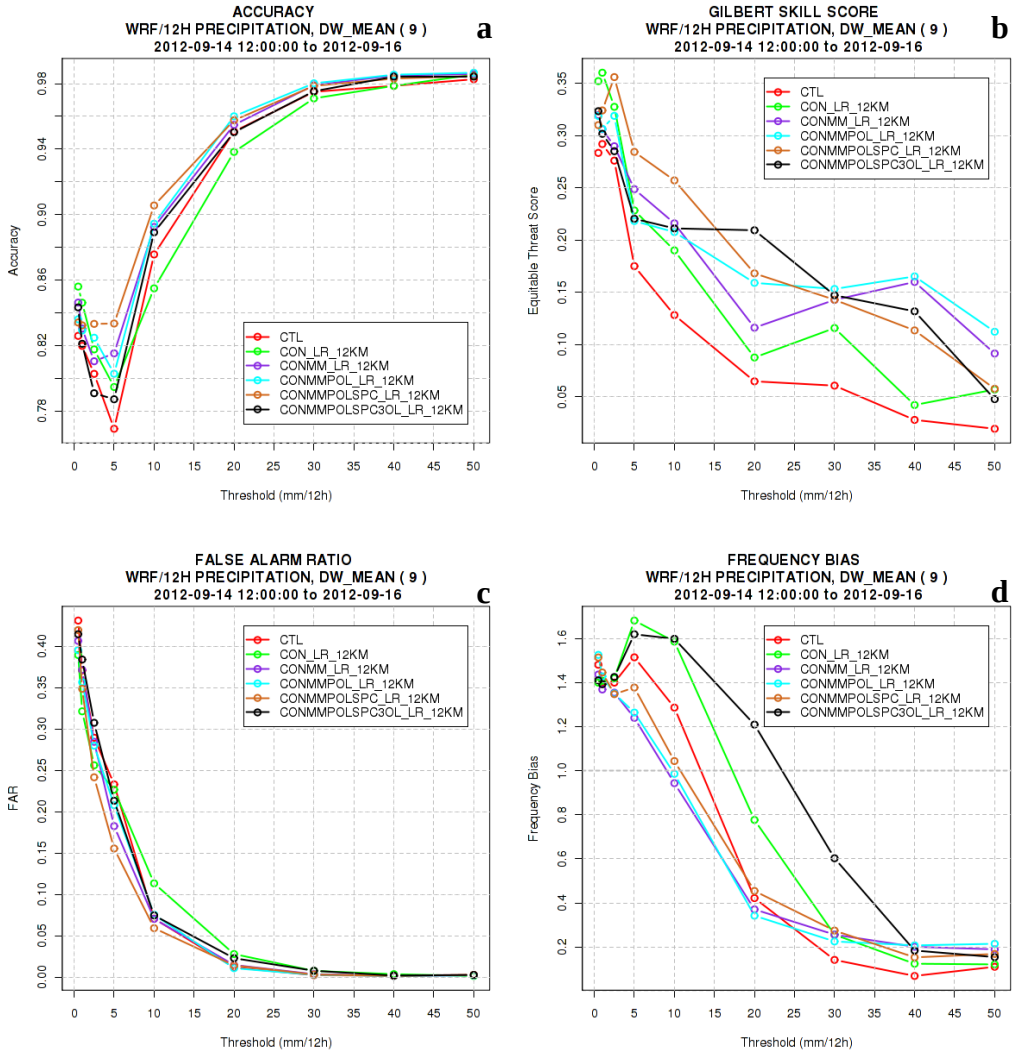


**Figure 7: Forecast Accuracy (a), Equitable Threat Score (b), False Alarm Ratio (c) and Frequency Bias (d) as a function of threshold. The red curve indicates CTL experiment, the green curve CON_LR_12KM, the blue curve CONMM_LR_12KM, the cyan curve CONMMPOL_LR_12KM, the brown curve CONMMPOLSPC_LR_12KM, the black curve CONMMPOLSPC3OL_LR_12KM.**

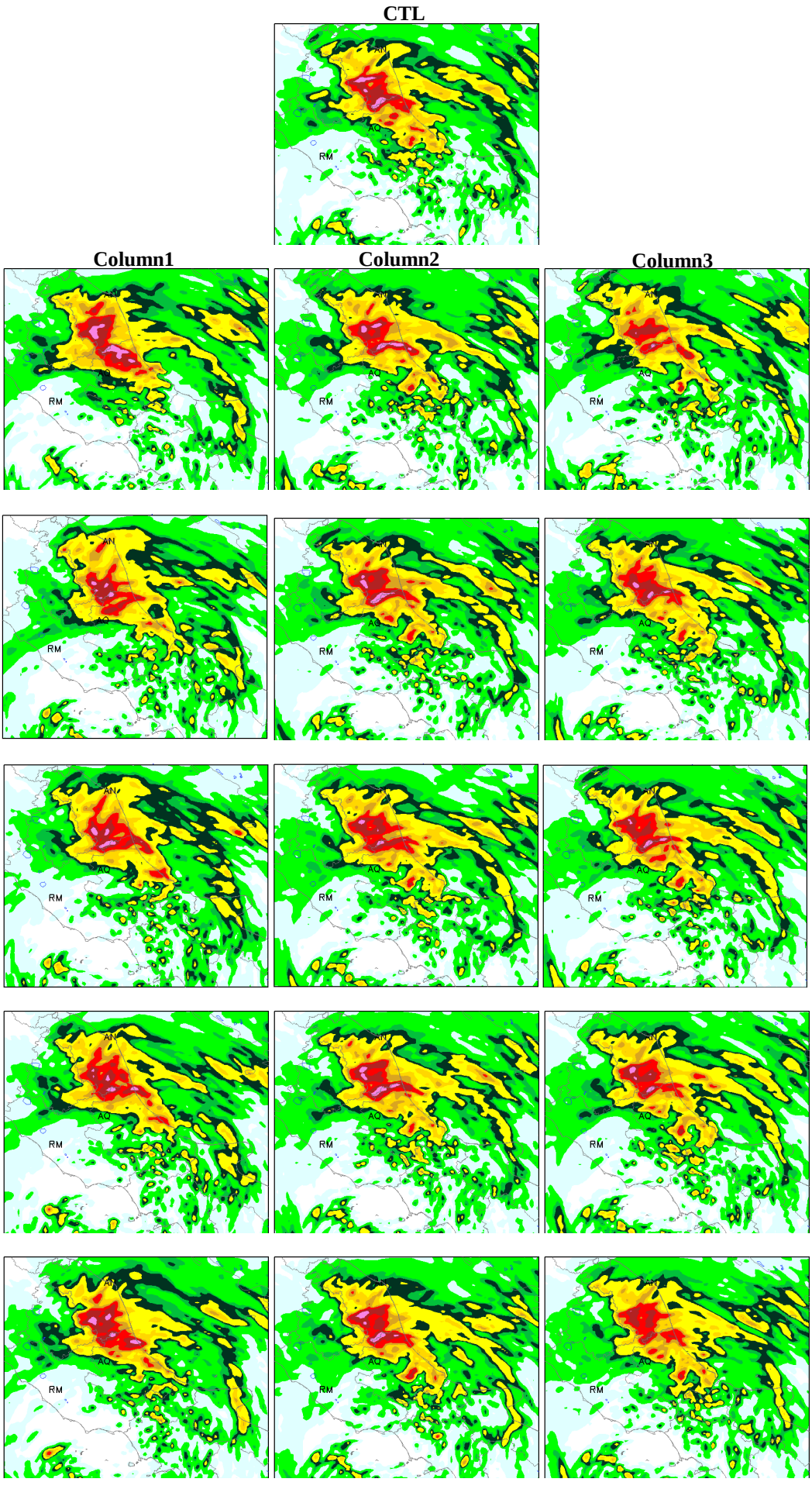
CTL
Column1
Column2
Column3
Line1
Line2
Line3
Line4
Line5


**Figure 8: WRF D02 accumulated 24h rainfall forecast over central Italy from 00:00UTC of 14 September 2012: CTL simulation (top center); on each column simulations obtained performing reflectivity assimilation at different resolutions (*12KM, *3KM, *12KM_3KM); on each line simulations performed assimilating different kinds of data (CON*, CONMM*, CONMMPOL*,CONMMPOLSPC*, CONMMPOLSPC3OL*).**

**Table 1: Technical characteristics of the three radars whose reflectivity have been assimilated during IOP4.**

| Features | Units | MM radar | P55C radar | SPC radar |
|---|---|---|---|---|
| Owner | | CF Abruzzo Region | ISAC-CNR of Rome | Arpa Emilia Romagna |
| Location | | Monte Midia | Rome | San Pietro Capofiume |
| Latitude | [deg] | 42,057 | 41,840 | 44,6547 |
| Longitude | [deg] | 13,177 | 12,647 | 11,6236 |
| Height (a.s.l.) | [m] | 1760 | 130 | 31 |
| Doppler | | YES | YES | YES |
| Dual Polarization | | NO | YES | YES |
| Range Resolution | [m] | 500 | 75 | 250 |
| Temporal Resolution | [min] | 15 | 5 | 15 |
| Number of PPI scans | | 4 (0, 1, 2, 3) | 6 or 8 (0.6, 1.6, 2.6, 4.4, 6.2, 8.3, 11.0, 14.6) | 6 (0.53, 1.4, 2.3, 3.2, 4.15, 5.0) |
| Maximum Range | [Km] | 120 or 240 | 125 | 125 |

**Table 2: List of experiments to assess the cumulus parameterization.**

| Experiment | Cumulus | Grid Resolution | Assimilation Synop+Temp | Assimilation Radar |
|---|---|---|---|---|
| KF_MYJ | KAIN-FRITSCH | 12KM/3KM | NO | NO |
| GRELL3D_MYJ | GRELL3D | 12KM/3KM | NO | NO |
| GRELL3D_MYJ_CUGD (CTL) | GRELL3D+CUGD | 12KM/3KM | NO | NO |

**Table 3: List of experiments to test the impact of data assimilation.**

| Experiment | Cumulus | Grid Resolution | Assimilation Synop+Temp | Assimilation Radar |
|---|---|---|---|---|
| CTL | GRELL3D+CUGD | 12KM/3KM | NO | NO |

| | | | | |
|---|---|---|---|---|
| CON | GRELL3D+CUGD | 12KM/3KM/BOTH | YES | NO |
| CONMM | GRELL3D+CUGD | 12KM/3KM/BOTH | YES | MM |
| CONMMPOL | GRELL3D+CUGD | 12KM/3KM/BOTH | YES | MM+POL |
| CONMMPOLSPC | GRELL3D+CUGD | 12KM/3KM/BOTH | YES | MM+POL+SPC |
| CONMMPOLSPC3OL | GRELL3D+CUGD | 12KM/3KM/BOTH | YES | MM+POL+SPC<br>with 3 outer loops |

**Table 4: Statistics referred to experiments in column 1: Forecast Accuracy (ACC), Frequency Bias (FBIAS), Equitable Threat Score (ETS), False Alarm Ratio (FAR) are considered as a function of thresholds (1mm/12h and 20mm/12h). The experiments are: CTL, CON_HR_12KM, CONMM_HR_12KM, CONMMPOL_HR_12KM, CONMMPOLSPC_HR_12KM, CONMMPOLSPC3OL_HR_12KM.**

| **Experiment** | **ACC** ***Thresholds mm/12h*** | | **FBIAS** ***Thresholds mm/12h*** | | **ETS** ***Thresholds mm/12h*** | | **FAR** ***Thresholds mm/12h*** | |
|---|---|---|---|---|---|---|---|---|
| | ***1*** | ***20*** | ***1*** | ***20*** | ***1*** | ***20*** | ***1*** | ***20*** |
| CTL | 0.83 | 0.94 | 0.94 | 1.13 | 0.33 | 0.19 | 0.21 | 0.03 |
| CON_HR_12KM | 0.81 | 0.93 | 0.91 | 1.12 | 0.25 | 0.17 | 0.26 | 0.04 |
| CONMM_HR_12KM | 0.82 | 0.94 | 0.95 | 0.99 | 0.28 | 0.17 | 0.24 | 0.03 |
| CONMMPOL_HR_12KM | 0.80 | 0.95 | 0.82 | 0.61 | 0.20 | 0.10 | 0.25 | 0.02 |
| CONMMPOLSPC_HR_12KM | 0.82 | 0.94 | 0.86 | 0.92 | 0.28 | 0.14 | 0.21 | 0.03 |
| CONMMPOLSPC3OL_HR_12KM | 0.82 | 0.95 | 0.93 | 0.84 | 0.30 | 0.16 | 0.20 | 0.03 |

**Table 5: Statistics referred to experiments in column 2: Forecast Accuracy (ACC), Frequency Bias (FBIAS), Equitable Threat Score (ETS), False Alarm Ratio (FAR) are considered as a function of thresholds (1mm/12h and 20mm/12h). The experiments are: CTL, CON_3KM, CONMM_3KM, CONMMPOL_3KM, CONMMPOLSPC_3KM, CONMMPOLSPC3OL_3KM.**

| **Experiment** | **ACC** ***Thresholds mm/12h*** | | **FBIAS** ***Thresholds mm/12h*** | | **ETS** ***Thresholds mm/12h*** | | **FAR** ***Thresholds mm/12h*** | |
|---|---|---|---|---|---|---|---|---|
| | ***1*** | ***20*** | ***1*** | ***20*** | ***1*** | ***20*** | ***1*** | ***20*** |
| CTL | 0.83 | 0.94 | 0.94 | 1.13 | 0.33 | 0.19 | 0.21 | 0.03 |
| CON_3KM | 0.82 | 0.94 | 0.80 | 0.83 | 0.24 | 0.15 | 0.22 | 0.03 |
| CONMM_3KM | 0.82 | 0.94 | 0.96 | 0.96 | 0.26 | 0.17 | 0.24 | 0.03 |
| CONMMPOL_3KM | 0.81 | 0.95 | 0.94 | 0.84 | 0.23 | 0.11 | 0.24 | 0.03 |
| CONMMPOLSPC_3KM | 0.82 | 0.94 | 1.03 | 0.90 | 0.28 | 0.16 | 0.24 | 0.03 |

| | | | | | | | | |
|---|---|---|---|---|---|---|---|---|
| CONMMPOLSPC3OL_3KM | 0.83 | 0.95 | 0.96 | 0.91 | 0.27 | 0.18 | 0.27 | 0.03 |

**Table 6: Statistics referred to experiments in column 3: Forecast Accuracy (ACC), Frequency Bias (FBIAS), Equitable Threat Score (ETS), False Alarm Ratio (FAR) are considered as a function of thresholds (1mm/12h and 20mm/12h). The experiments are: CTL, CON_12KM_3KM, CONMM_12KM_3KM, CONMMPOL_12KM_3KM, CONMMPOLSPC_12KM_3KM, CONMMPOLSPC3OL_12KM_3KM.**

| Experiment | ACC *Thresholds mm/12h* | | FBIAS *Thresholds mm/12h* | | ETS *Thresholds mm/12h* | | FAR *Thresholds mm/12h* | |
|---|---|---|---|---|---|---|---|---|
| | *1* | *20* | *1* | *20* | *1* | *20* | *1* | *20* |
| CTL | 0.83 | 0.94 | 0.94 | 1.13 | 0.33 | 0.19 | 0.21 | 0.03 |
| CON_12KM_3KM | 0.81 | 0.95 | 0.84 | 0.73 | 0.20 | 0.14 | 0.27 | 0.02 |
| CONMM_12KM_3KM | 0.83 | 0.94 | 0.96 | 0.94 | 0.28 | 0.16 | 0.23 | 0.03 |
| CONMMPOL_12KM_3KM | 0.81 | 0.95 | 0.96 | 0.75 | 0.23 | 0.13 | 0.25 | 0.03 |
| CONMMPOLSPC_12KM_3KM | 0.81 | 0.95 | 1.04 | 0.79 | 0.26 | 0.17 | 0.28 | 0.02 |
| CONMMPOLSPC3OL_12KM_3KM | 0.83 | 0.95 | 0.98 | 0.73 | 0.30 | 0.18 | 0.25 | 0.02 |

**Table 7: Statistics referred to experiments in line 1: Forecast Accuracy (ACC), Frequency Bias (FBIAS), Equitable Threat Score (ETS), False Alarm Ratio (FAR) are considered as a function of thresholds (1mm/12h and 20mm/12h). The experiments are: CTL, CON_3KM, CON_HR_12KM, CON_12KM_3KM.**

| Experiment | ACC *Thresholds mm/12h* | | FBIAS *Thresholds mm/12h* | | ETS *Thresholds mm/12h* | | FAR *Thresholds mm/12h* | |
|---|---|---|---|---|---|---|---|---|
| | *1* | *20* | *1* | *20* | *1* | *20* | *1* | *20* |
| CTL | 0.83 | 0.94 | 0.94 | 1.13 | 0.33 | 0.19 | 0.21 | 0.03 |
| CON_3KM | 0.82 | 0.94 | 0.80 | 0.83 | 0.24 | 0.15 | 0.22 | 0.03 |
| CON_HR_12KM | 0.81 | 0.93 | 0.91 | 1.12 | 0.25 | 0.17 | 0.26 | 0.04 |
| CON_12KM_3KM | 0.81 | 0.95 | 0.84 | 0.73 | 0.20 | 0.14 | 0.27 | 0.02 |

**Table 8: Statistics referred to experiments in line 2: Forecast Accuracy (ACC), Frequency Bias (FBIAS), Equitable Threat Score (ETS), False Alarm Ratio (FAR) are considered as a function of thresholds (1mm/12h and 20mm/12h). The experiments are: CTL, CONMM_3KM, CONMM_HR_12KM, CONMM_12KM_3KM.**

| Experiment | ACC *Thresholds mm/12h* | | FBIAS *Thresholds mm/12h* | | ETS *Thresholds mm/12h* | | FAR *Thresholds mm/12h* | |
|---|---|---|---|---|---|---|---|---|
| | *1* | *20* | *1* | *20* | *1* | *20* | *1* | *20* |
| CTL | 0.83 | 0.94 | 0.94 | 1.13 | 0.33 | 0.19 | 0.21 | 0.03 |
| CONMM_3KM | 0.82 | 0.94 | 0.96 | 0.96 | 0.26 | 0.17 | 0.24 | 0.03 |

| | | | | | | | | |
|---|---|---|---|---|---|---|---|---|
| CONMM_HR_12KM | 0.82 | 0.94 | 0.95 | 0.99 | 0.28 | 0.17 | 0.24 | 0.03 |
| CONMM_12KM_3KM | 0.83 | 0.94 | 0.96 | 0.94 | 0.28 | 0.16 | 0.23 | 0.03 |

**Table 9: Statistics referred to experiments in line 3: Forecast Accuracy (ACC), Frequency Bias (FBIAS), Equitable Threat Score (ETS), False Alarm Ratio (FAR) are considered as a function of thresholds (1mm/12h and 20mm/12h). The experiments are: CTL, CONMMPOL_3KM, CONMMPOL_HR_12KM, CONMMPOL_12KM_3KM.**

| Experiment | ACC *Thresholds mm/12h* | | FBIAS *Thresholds mm/12h* | | ETS *Thresholds mm/12h* | | FAR *Thresholds mm/12h* | |
|---|---|---|---|---|---|---|---|---|
| | *1* | *20* | *1* | *20* | *1* | *20* | *1* | *20* |
| CTL | 0.83 | 0.94 | 0.94 | 1.13 | 0.33 | 0.19 | 0.21 | 0.03 |
| CONMMPOL_3KM | 0.81 | 0.95 | 0.94 | 0.84 | 0.23 | 0.11 | 0.24 | 0.03 |
| CONMMPOL_HR_12KM | 0.80 | 0.95 | 0.82 | 0.61 | 0.20 | 0.10 | 0.25 | 0.02 |
| CONMMPOL_12KM_3KM | 0.81 | 0.95 | 0.96 | 0.75 | 0.23 | 0.13 | 0.25 | 0.03 |

**Table 10: Statistics referred to experiments in line4: Forecast Accuracy (ACC), Frequency Bias (FBIAS), Equitable Threat Score (ETS), False Alarm Ratio (FAR) are considered as a function of thresholds (1mm/12h and 20mm/12h). The experiments are: CTL, CONMMPOLSPC_3KM, CONMMPOLSPC_HR_12KM, CONMMPOLSPC_12KM_3KM.**

| Experiment | ACC *Thresholds mm/12h* | | FBIAS *Thresholds mm/12h* | | ETS *Thresholds mm/12h* | | FAR *Thresholds mm/12h* | |
|---|---|---|---|---|---|---|---|---|
| | *1* | *20* | *1* | *20* | *1* | *20* | *1* | *20* |
| CTL | 0.83 | 0.94 | 0.94 | 1.13 | 0.33 | 0.19 | 0.21 | 0.03 |
| CONMMPOLSPC_3KM | 0.82 | 0.94 | 1.03 | 0.90 | 0.28 | 0.16 | 0.25 | 0.03 |
| CONMMPOLSPC_HR_12KM | 0.82 | 0.94 | 0.86 | 0.92 | 0.28 | 0.14 | 0.21 | 0.03 |
| CONMMPOLSPC_12KM_3KM | 0.81 | 0.95 | 1.04 | 0.79 | 0.26 | 0.17 | 0.28 | 0.02 |

**Table 11: Statistics referred to experiments in line 5: Forecast Accuracy (ACC), Frequency Bias (FBIAS), Equitable Threat Score (ETS), False Alarm Ratio (FAR) are considered as a function of thresholds (1mm/12h and 20mm/12h). The experiments are: CTL, CONMMPOLSPC3OL_3KM, CONMMPOLSPC3OL_HR_12KM, CONMMPOLSPC3OL_12KM_3KM.**

| Experiment | ACC *Thresholds mm/12h* | | FBIAS *Thresholds mm/12h* | | ETS *Thresholds mm/12h* | | FAR *Thresholds mm/12h* | |
|---|---|---|---|---|---|---|---|---|
| | *1* | *20* | *1* | *20* | *1* | *20* | *1* | *20* |
| CTL | 0.83 | 0.94 | 0.94 | 1.13 | 0.33 | 0.19 | 0.21 | 0.03 |
| CONMMPOLSPC3OL_3KM | 0.83 | 0.95 | 0.96 | 0.91 | 0.27 | 0.18 | 0.27 | 0.03 |
| CONMMPOLSPC3OL_HR_12KM | 0.82 | 0.95 | 0.93 | 0.84 | 0.30 | 0.16 | 0.20 | 0.03 |

| | | | | | | | | |
|---|---|---|---|---|---|---|---|---|
| CONMMPOLSPC3OL_12KM_3KM | 0.83 | 0.95 | 0.98 | 0.73 | 0.30 | 0.18 | 0.25 | 0.02 |

580